In the supporting information, the contents are organised as 1) tables, 2) figures, and 3) description of some procedures for LAAPTOF data analysis as well as the corresponding equations and uncertainties.

Table S1: Overview of laboratory generated aerosol particles for reference mass spectra

Aerosol particle types	Size/nm		Morphology	Source	Generation	No. of
	d_{va}	width[a]			method	spectra
1. Particles consisting of pure compounds						
Ammonium nitrate, NH_4NO_3	1160	101	aspherical	≥ 99.5%, Fluka	A	497
Ammonium sulfate[b], $(NH_4)_2SO_4$	611	79	aspherical	≥ 99.5%, Merck	A	537
Potassium sulfate, K_2SO_4	1465	232	aspherical	≥ 99%, Merck	A	300
Sodium chloride, NaCl	1202	133	cubic	≥ 99.5%, Merck	A	250
Silica, SiO_2 (Glass beads)	2097	44	spherical	Palas GmbH	S	347
Oxalic acid, $C_2H_4O_2$	1081	322	spherical	Merck	A	773
Pinic acid, $C_9H_{14}O_4$	902	94	spherical	University of Mainz	A	683
Cis-pinonic acid, $C_{10}H_{16}O_3$	702	88	spherical	98%, ACROS ORGANICS	A	600
Humic acid	1221	126	spherical	100%, Alfa Aesar	A	773
Polystyrene latex (PSL) (d_m=800nm)	818	3	spherical	Thermo scientific	A	235
2. Particles consisting of well-defined mixtures						
Ammonium nitrate & ammonium sulfate (mass ratio = 1:1)	1102	165	aspherical	single component samples are from the same source	A	454
Potassium sulfate & sodium chloride (mass ratio = 1:1)	1375	197	aspherical	as the corresponding pure compounds		259
Ammonium nitrate & potassium sulfate (mass ratio = 2:1)	854	112	aspherical			576
Hematite	1091	817	spherical	Karlsruhe Institute of Technology (KIT)	A	320
Pure sea salt	1205	218	cubic	Sigma Aldrich	B1	422
α-Pinene secondary organic aerosols (SOA)	505	84	spherical	(1S)-(-)-α-pinene (99%) from Aldrich	B1[c]	1938
Potassium sulfate coated PSL(d_m=800nm)	805	58	partially coated	Merck & Thermo scientific	A	609
Poly(allylamine hydrochloride) coated gold	400[d]		300 nm core-50 nm shell	Nanopartz Inc.	Nebulized without sizing	417
3. Particles consisting of complex mixtures						
Soot1 with low organic carbon	386[e]	275	agglomerates	incomplete combustion of propane, C/O=0.29	B2	617
Soot1 with high organic carbon	120[e]	58	agglomerates	incomplete combustion of propane, C/O=0.54	B2	347
Soot2 Lignocellulosic char	828	766	agglomerates	Lignocellulosic char from Chestnut wood; University of Zürich, Switzerland	S	390
Soot3 Diesel particles	624±980[f]		agglomerates	NIST (2975)	S	533
Arizona test dust	1169	874	aspherical	Powder Technology Inc.	S	261
Saharan desert dust 1 (Morocco)	890	1230	aspherical	Konrad Kandler, TU Darmstadt	S	338
Saharan desert dust 2 (Cairo)	1334±1454[f]		aspherical	Khaled Megahed, KIT	S	396
Arable soil dust SDGe01 (Gottesgabe, Germany)	912	392	aspherical	Roger Funk[g]	B1[h]	583
Arable soil dust SDPA01 (Paulinenaue, Germany)	787	334	aspherical	Roger Funk[g]	B1[h]	385
Arable soil dust SDAr08 (Argentina)	910	407	aspherical	Roger Funk[g]	B1[h]	592
Arable soil dust SDWY01 (Wyoming, USA)	864	430	aspherical	Tom Hill[i]	B1[h]	623
Agricultural soil dust (Northern Germany)	561	249	aspherical	Roger Funk[g]	B1[h]	583
Urban dust	1329	1266	aspherical	NIST(1649a)	A	375
Illite_NX	825	260	sheet	Arginotec	A	807
Sea salt with skeletonema marinoi [j]	1212	338	cubic	Matt Salter[j]	B1	526

Note: "DMA" is short for Differential Mobility Analyzer; "AIDA" is short for Aerosol Interactions and Dynamics in the Atmosphere; spectra number is the number of averaged spectra. For aerosol generation methods: "A" represents for the method by using a nebulizer and a DMA (refer to setup A in Fig. 1); "B1" and "B2" represent the methods in which particles were sampled from AIDA and a stainless steel cylinder, respectively (refer to setup B in Fig. 1); "S" corresponds to particles mobilized by shaking in a reservoir.

[a]: These values represent the standard deviation from Gaussian fitting to the measured particle sizes (d_{va}).

[b]: There is only one weak but reproducible peak m/z 30 NO^+ in the positive spectra.

[c]: SOA particles were formed in the Aerosol Preparation and Characterization (APC) chamber and then transferred into the AIDA chamber.

[d]: The nominal geometric size given by the manufacture Nanopartz Inc.

[e]: Electrical mobility equivalent diameter, d_m, measured by a scanning mobility particle sizer (SMPS).

[f]: The sizes (d_{va}) of Diesel particles and Saharan desert dust 2 are average values with their standard deviation.

[g]: Institute of Soil Landscape Research, Leibniz Centre for Agricultural Landscape Research, Germany.

[h]: Soil dust samples were dispersed by a rotating brush generator and injected via cyclones into the AIDA chamber.

[i]: Department of Atmospheric Science, Colorado State University, Fort Collins, Colorado, USA.

[j]: Samples, provided by Elena Gorokhova and Matt Salter at Stockholm University, they were prepared by diluting a pure skeletonema marinoi culture with artificial seawater (sigma sea salt) to conditions representative of a bloom in the ocean.

19   **Table S2: Summary of peak assignments**

	Cations				Anions		
m/z	carbon	inorganic	organic	m/z	carbon	inorganic	organic
7+		Li^+		1-		H^-	
12+	C^+			8-		O^{2-}	
13+			CH^+	12-	C^-		
15+			CH_3^+/NH^+	16-		O^-	
17+		OH^+		17-		OH^-	
18+		NH_4^+/H_2O^+		24-	C_2^-		
23+		Na^+		25-			C_2H^-
24+	C_2^+	Mg^+		26-			$CN/C_2H_2^-$
27+		Al^+	$C_2H_3^+$	32-		S^-	
28+		Si^+	CO^+	36-	C_3^-		
29+			$C_2H_5^+/CHO^+$	35-		Cl^-	
30+		NO^+	CH_3NH^+/CH_2O^+	37-		Cl^-	
36+	C_3^+			42-			$CNO/C_2H_2O^-$
39+		K^+	$C_3H_3^+$	43-		AlO^-	
40+		Ca^+	C_2O^+	45-			$COOH^-$
41+		K^+	$C_3H_5^+$	46-		NO_2^-	
43+			$C_3H_7^+/C_2H_3O^+$	48-	C_4^-	SO^-	
44+		SiO^+	CO_2^+	59-		AlO_2^-	CH_2COOH^-
46+		NO_2^+		60-	C_5^-	SiO_2^-	
48+	C_4^+			62-		NO_3^-	
51+			$C_4H_3^+$	63-		PO_2^-	
53+			$C_4H_5^+$	64-		SO_2^-	
54+		Fe^+		70-		$^{35}Cl_2^-$	
55+		Mn^+	$C_4H_7^+/C_3H_3O^+$	71-			CCH_2COOH^-
56+		$Fe/CaO/Si_2^+$	$C_4H_8^+$	72-	C_6^-	FeO^-	
57+		$CaOH^+$	$C_4H_9^+/C_2OOH^+$	73-			$C_2H_4COOH^-$
58+		Ni^+	$C_2H_5-NH-CH_2^+$	76-		SiO_3^-	
59+			$(CH_3)_3N^+$	77-		$HSiO_3^-$	
60+	C_5^+			79-		PO_3^-	
63+		Cu^+	$C_5H_3^+$	80-		SO_3^-	
64+		Zn^+		81-		HSO_3^-	
65+		Cu^+		84-	C_7^-		
66+		Zn^+		85-			$C_3H_4COOH^-$
69+			$C_5H_9^+$	86-		FeO_2^-	
71+			$C_4H_7O^+$	88-		$Si_2O_2^-/FeO_2^-$	
72+	C_6^+			89-			$(CO)_2OOH^-$
77+			$C_6H_5^+$	93-		$NaCl_2^-$	
81+		Na_2Cl^+	$C_6H_9^+$	95-		$NaCl_2^-/PO_4^-$	
83+		Na_2Cl^+	$C_5H_7O^+$	96-	C_8^-	SO_4^-	
84+	C_7^+			97-		HSO_4^-	
85+			$C_7H_5^+/C_3HO_3^+$	99-			$C_4H_6COOH^-$
88+		FeO_2^+		103-		$(AlO)SiO_2^-$	
91+			$C_7H_7^+$	108-	C_9^-		
95+			$C_7H_{11}^+$	109-		KCl_2^-	
96+	C_8^+	Ca_2O^+		117-			$(CO)_3OOH^-$
97+		$KNaCl^+$	$C_4HO_3^+$	119-		$AlSiO_4^-/NaSiO_4^-$	
103+			$C_8H_7^+$	130-		$NaCl_3^-$	
105+			$C_8H_9^+$	135-		KSO_4^-	
108+	C_9^+			136-		$(SiO_2)_2O^-/KHSO_4^-$	
112+		$(CaO)_2^+$		148-		$(SiO_2)_2Si^-$	
113+		K_2Cl^+		151-		$Na_2Cl_3^-$	
115+		K_2Cl^+	$C_9H_7^+$	153-		$Na_2Cl_3^-$	
120+	C_{10}			179-		$AlSiO_4.SiO_2^-$	
132+	C_{11}^+						
206–208+		Pb^+					

20

21 **Table S3: Codes for reference particle types used for classification by using the reference-spectra based method**

positive code	reference particle	negative code	reference particle
01	Ammonium Nitrate (AN)	01	Ammonium Nitrate and Sulfate (AN+AS)
02	Pinonic Acid (PinoA)	02	Ammonium Nitrate and Potassium Sulfate (AN+PS)
03	Oxalic Acid (OA)	03	Desert Dust (Morroco) (MD)
04	Ammonium Nitrate and Potassium Sulfate (AN+PS)	04	Urban Dust (UD)
05	Potassium Sulfate Coated PSL (PSL+PS)	05	Arable Soil Dust (German) (SDGe01)
06	Agricultural Soil Dust (ASD)	06	Diesel Soot (DS)
07	Diesel Soot (DS)	07	Biomass Burning Soot (BS)
08	Biomass Burning Soot (BS)		
09	Sea salt (pure) (SS)		
10	Fuzzy Class 6_Calcium rich		

22

23 Note: In order to minimize the complexity, the reference number was reduced by observing the histogram of particle types based on the

24 correlation between each ambient spectrum (7314 in total) and our 32 laboratory based reference spectra relevant for atmospheric aerosol

25 (refer to the details of reference spectra-oriented grouping procedure after Fig. S13 in the supplementary information).

26
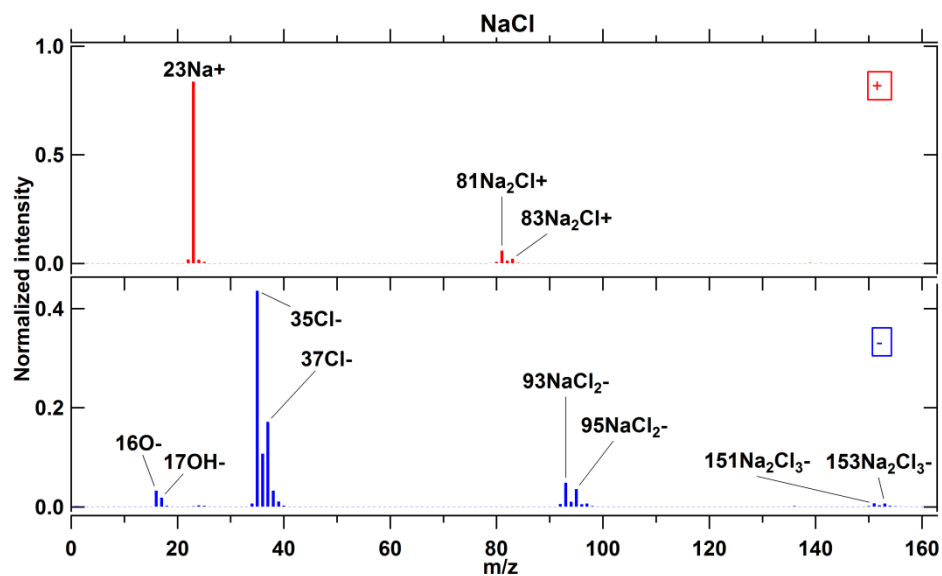
27 **Figure S1: Average mass spectrum for 1170 nm (d$_{va}$) pure NaCl particles. The ratio of m/z 35 Cl$^-$ to m/z 37 Cl$^-$ is ~3.2, similar as the**
28 **natural isotopic ratio of ~3.1 for ^{35}Cl/^{37}Cl. 250 single particle mass spectra were averaged for this spectrum.**

29

30

31
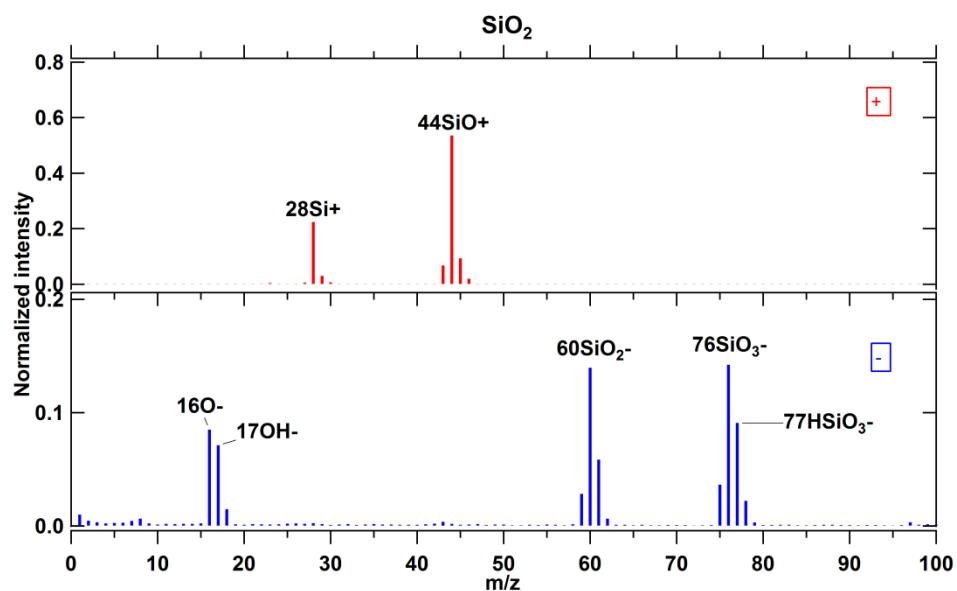
32 **Figure S2: Average mass spectrum for 2097 nm (d$_{va}$) SiO$_2$ particles (glass beads). The ratio of m/z 44 SiO$^+$ to m/z 28 Si$^+$ is ~2.4; (m/z**
33 **76 SiO$_3^-$ + m/z 77 HSiO$_3^-$) to m/z 60 SiO$_2^-$ is ~1. Such peak ratios are typical for SiO$_2$ particles. 347 single particle mass spectra were**
34 **averaged for this spectrum.**
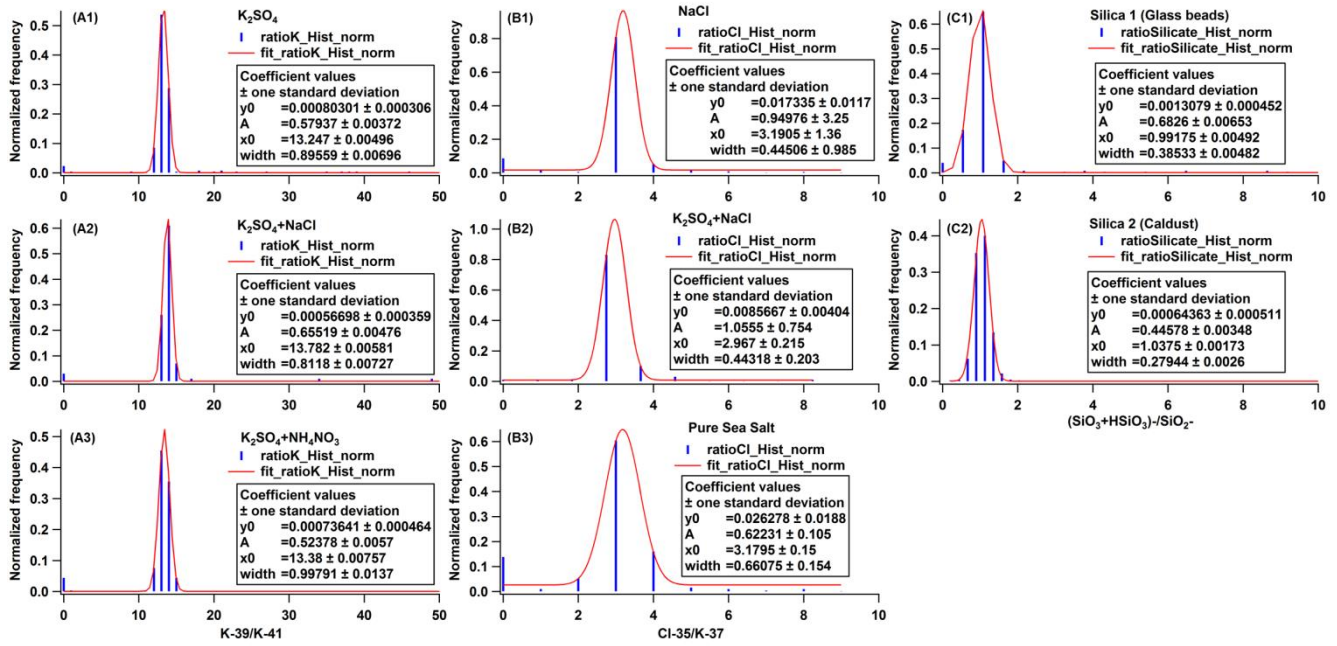
Figure S3: Histogram of peak ratios for different particle samples: panel A1 to A3 are for the isotopic ratio of K-39/K-41 arising from K containing samples; panel B1 to B3 are for the isotopic ratio of Cl-35/Cl-37 arising from Cl containing samples; panel C1 and C2 are for the peak ratio of $(SiO_3^-+HSiO_3^-)/SiO_2^-$ arising from silicate containing samples.

40
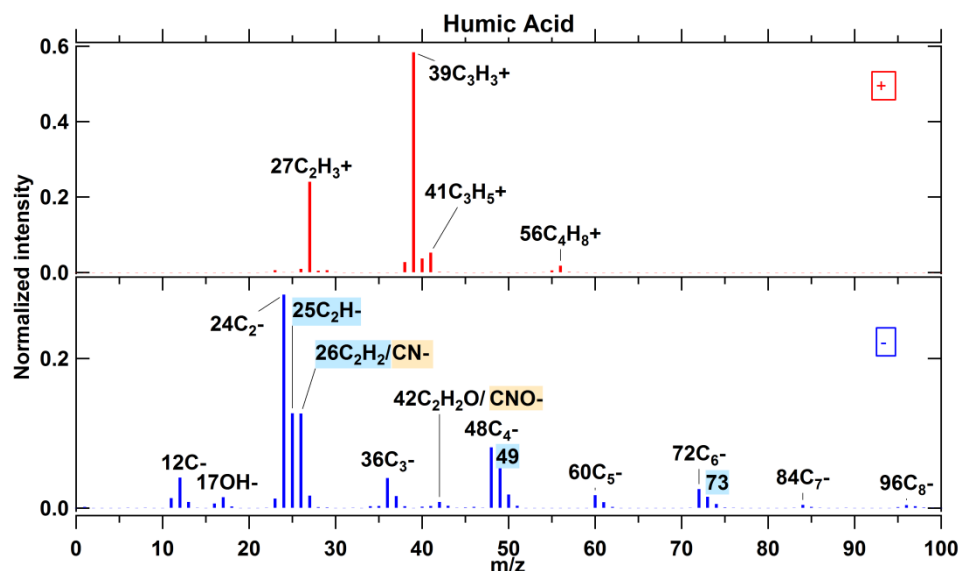
41 **Figure S4: Average mass spectrum for 1221 nm (d$_{va}$) humic acid particles. Fragments labelled in blue are typical for unsaturated**
42 **organic compounds; fragments labelled in orange are from nitrogen-containing organic compounds. 773 single particle mass spectra**
43 **were averaged for this spectrum.**

44

45

46
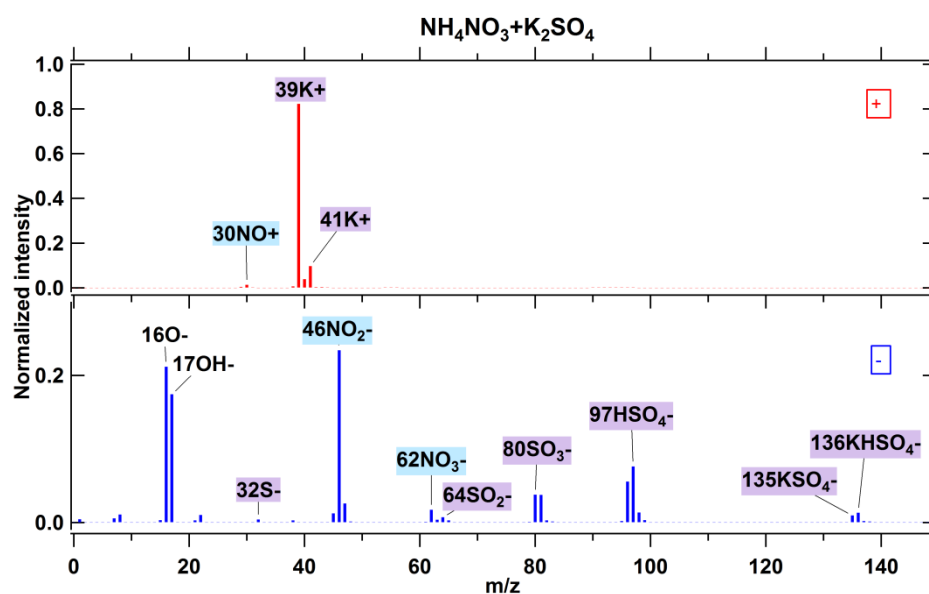
47 **Figure S5: Average mass spectrum for 854 nm (d$_{va}$) particles of homogeneous internal mixtures of inorganic compounds, NH$_4$NO$_3$**
48 **and K$_2$SO$_4$, 576 single spectra averaged. The blue and purple labels represent the fragments arising from pure NH$_4$NO$_3$ and pure**
49 **K$_2$SO$_4$ components, respectively.**
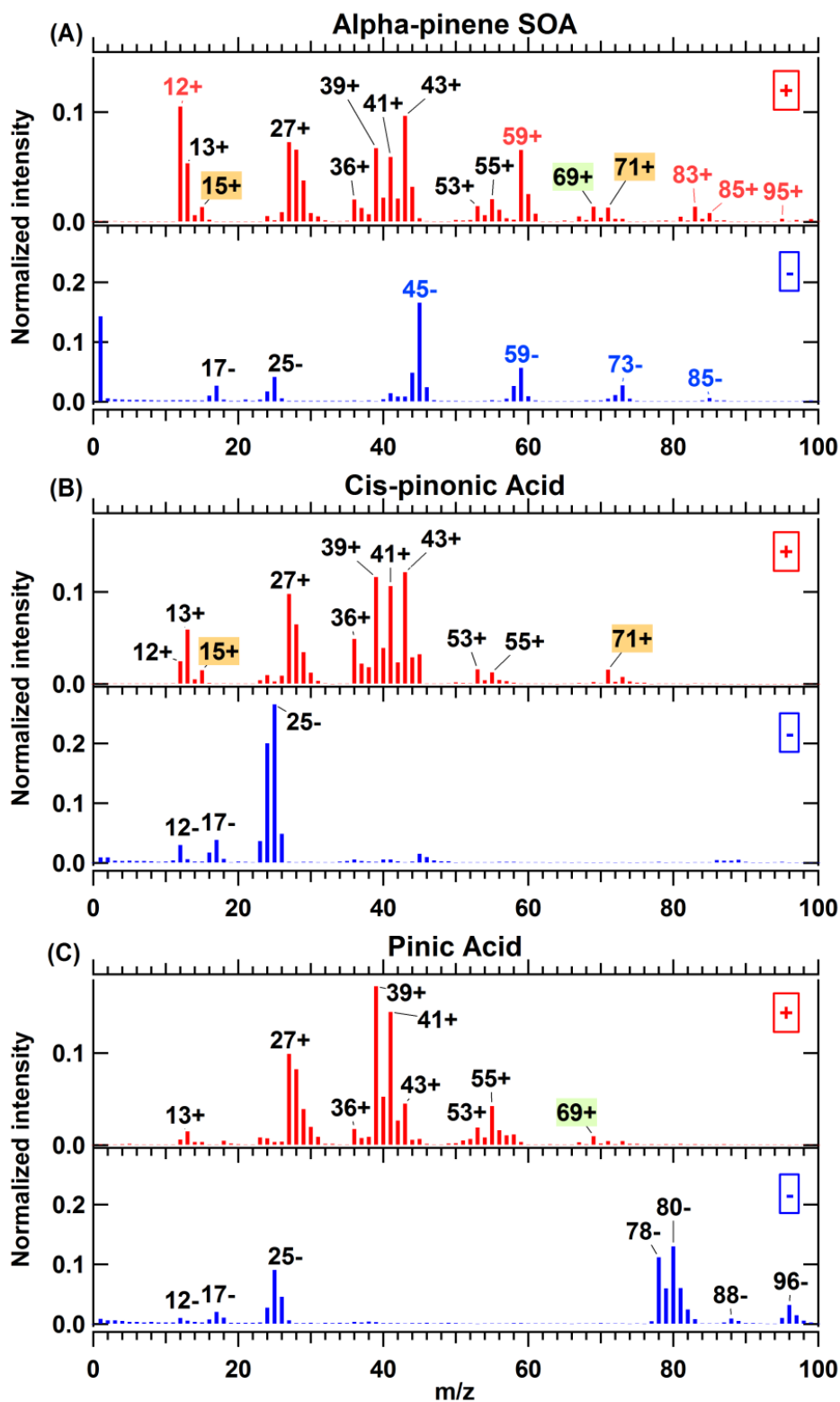
Figure S6: Average mass spectra for particles of homogeneous internal mixtures of (A) secondary organic aerosol (SOA) particles from α-pinene ozonolysis, which was performed in the APC chamber then the resulting particles were transferred into AIDA chamber at 263 K and 95% RH, d_{va}= 505 nm, 1938 single spectra averaged, as well as pure aerosol particles consisting of (B) cis-pinonic acid, d_{va}= 702 nm, 600 single spectra averaged and (C) pinic acid, d_{va}= 902 nm, 683 single spectra averaged. In panel (A), m/z 15[+] and 71[+] labelled in orange are arising from cis-pinonic acid, while m/z 69[+] labelled in green is arising from pinic acid.

56
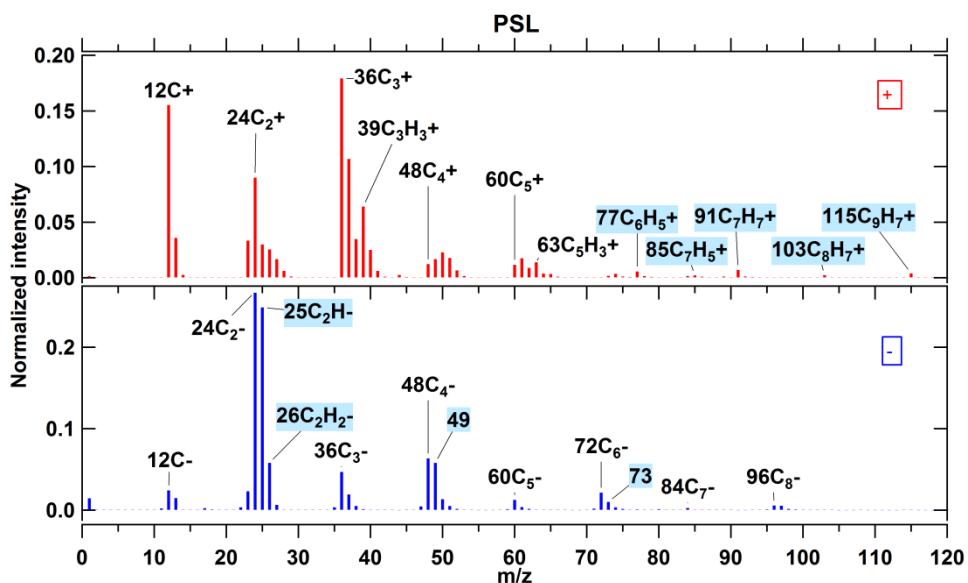
Figure S7: Average mass spectra for 818 nm (d_{va}) pure PSL. Fragments labelled in blue are typical patterns for aromatic compounds. 235 single particle mass spectra were averaged for this spectrum.

61
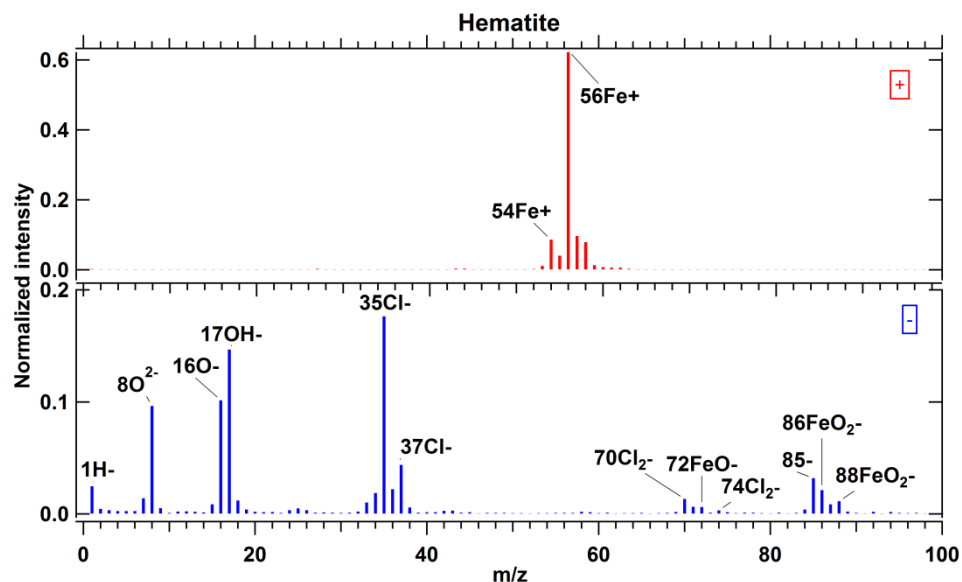
Figure S8: Average mass spectrum for 800 nm (geometric size) hematite particles, 320 single spectra averaged.

Hematite with signatures for iron (intensive m/z 56 Fe^+ and the other iron isotopes m/z 54, 57, and 58), oxides of iron (m/z 72 FeO^-, 86 FeO_2^-, and 88 FeO_2^-), and chlorides (m/z 35 Cl^-, 37 Cl^-, 70 Cl_2^-, and 74 Cl_2^-). Chloride ions observed originate from the hematite synthesis process. This is comparable to the hematite spectra measured by PALMS (Gallavardin et al., 2008).

66
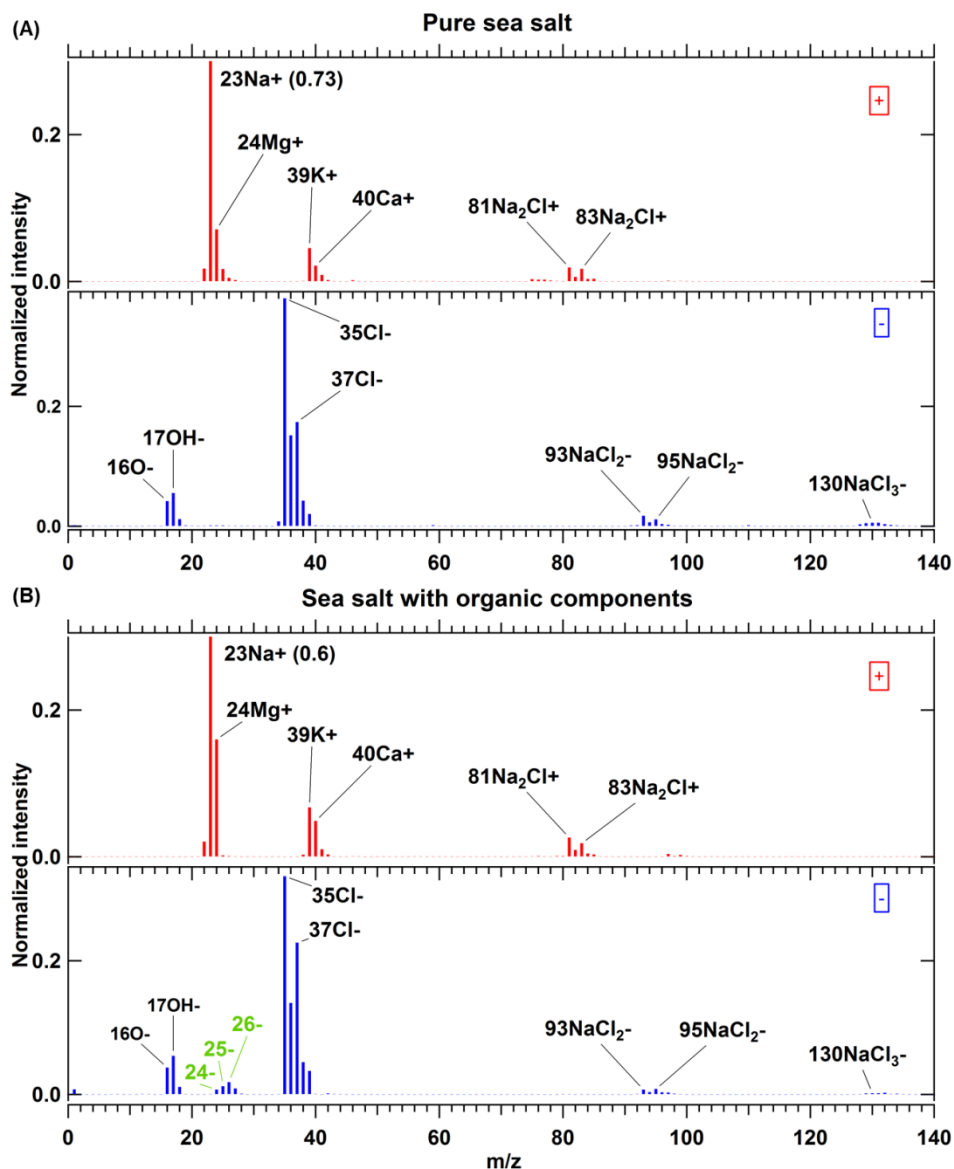
67 **Figure S9: Average mass spectra for (A) pure sea salt, 422 single spectra averaged, and (B) sea salt particles with skeletonema**
68 **marinoi (organic components), 526 single spectra averaged. These aerosol particles were sampled from the AIDA chamber at 246 K**
69 **and 75% RH, d_{va}= ~1200 nm. The numbers in brackets beside peaks 23$^+$ are the exact intensity values for them. In panel (B) obvious**
70 **organic signatures m/z 24$^-$, 25$^-$, and 26$^-$ labelled in green can be observed.**

71   Pure sea salt particles have signatures for NaCl (m/z 23$^+$, 81$^+$, 83$^+$, 35$^-$, 37$^-$, 93$^-$, and 95$^-$), and other metals (m/z 24 Mg$^+$,

72 39 K$^+$, and 40 Ca$^+$). Sea salt particles containing biological components have the signatures for pure sea salt as well as the

73 signatures for organic compounds (m/z 24$^-$, 25$^-$, and 26$^-$).
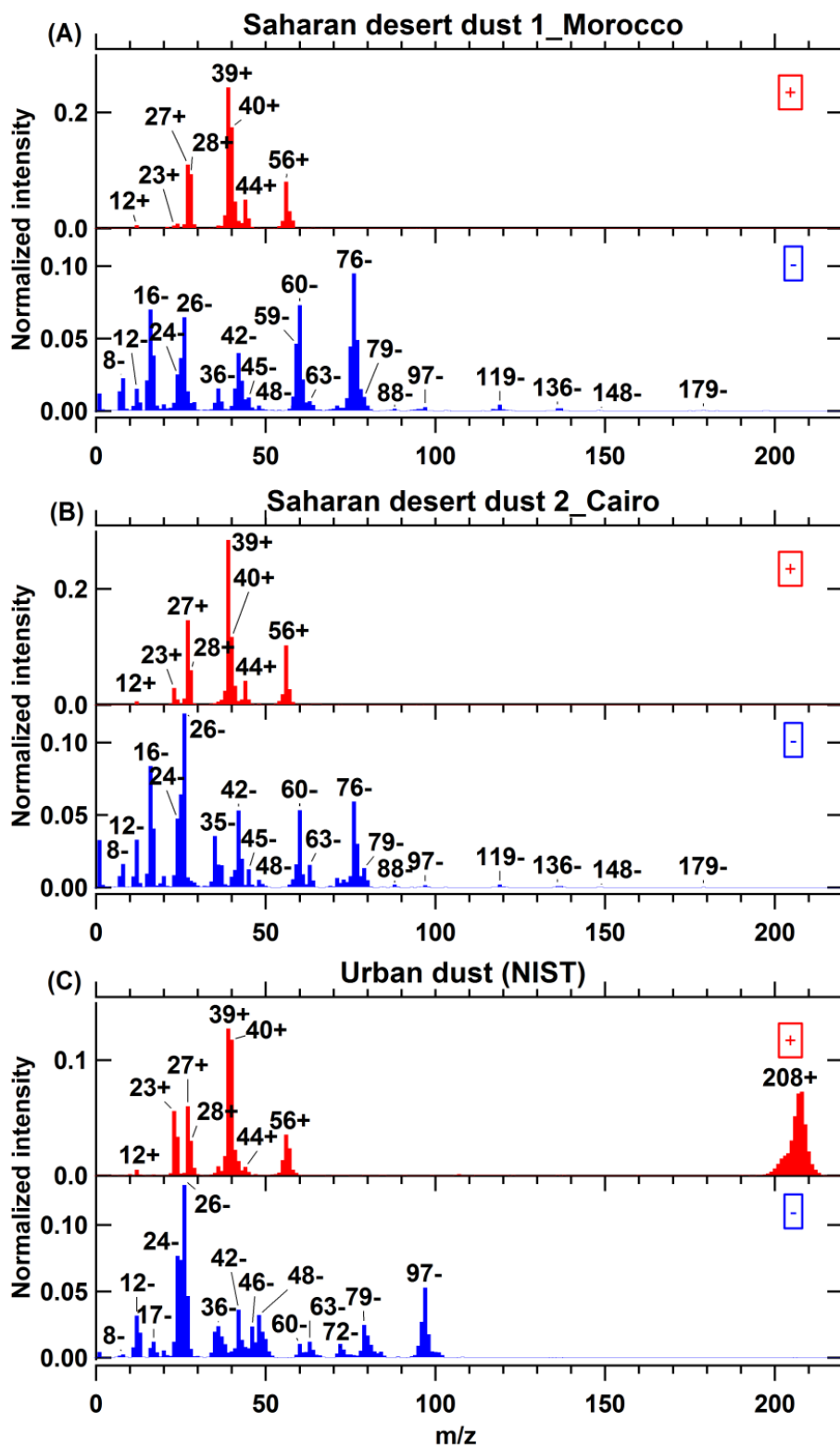
74
75 **Figure S10: Average mass spectra for Saharan desert dust from (A) Morocco, 338 single spectra averaged and (B) Cairo city, 396**
76 **single spectra averaged, and (C) urban dust (standard material from NIST), 375 single spectra averaged.**
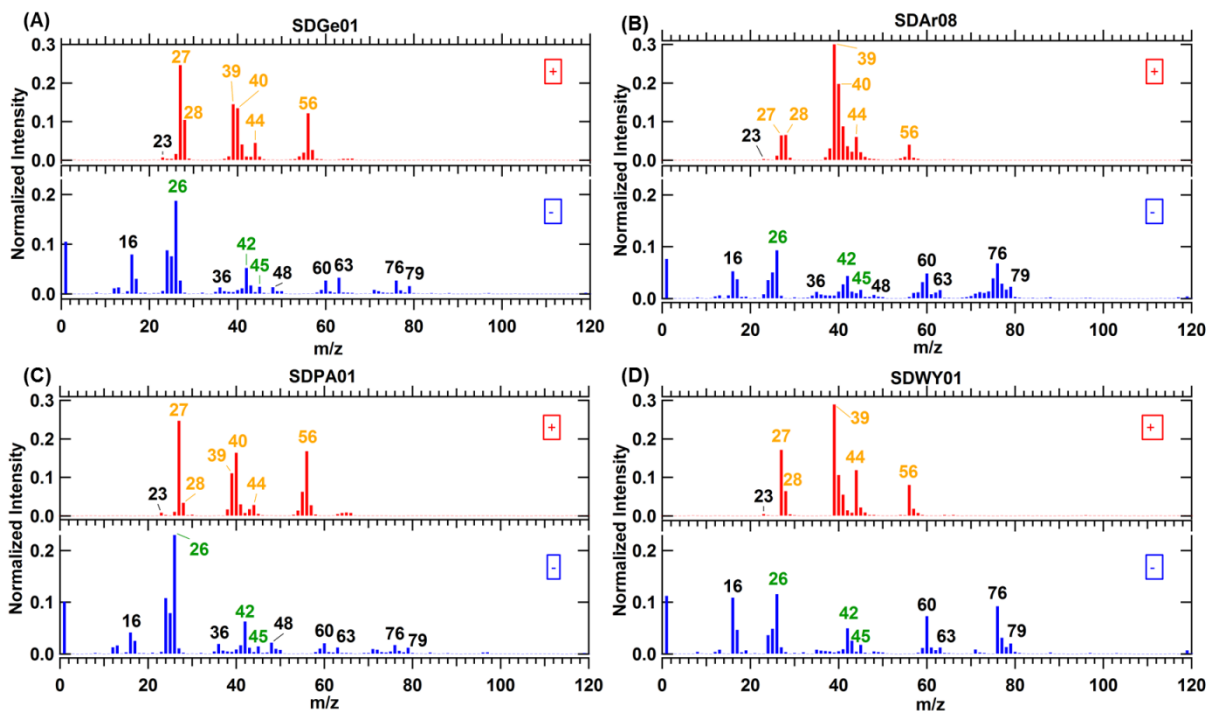
Figure S11: Average mass spectra for four different arable soil dusts sampled at two sites from Germany (SDGe01 is from Gottesgabe and SDPA01 is from Paulinenaue), Argentina (SDAr08), and Wyoming in USA (SDWY01). The corresponding aerosol particles were dispersed by a rotating brush generator and injected via cyclones into the AIDA chamber at 256 K and 80% RH. Black tags represent inorganic fragments; green tags represent organic fragments; orange tags represent fragments originating from inorganic and organic species. The numbers of spectra for each average spectrum are 583 (A), 592 (B), 385 (C) and 623 (D).
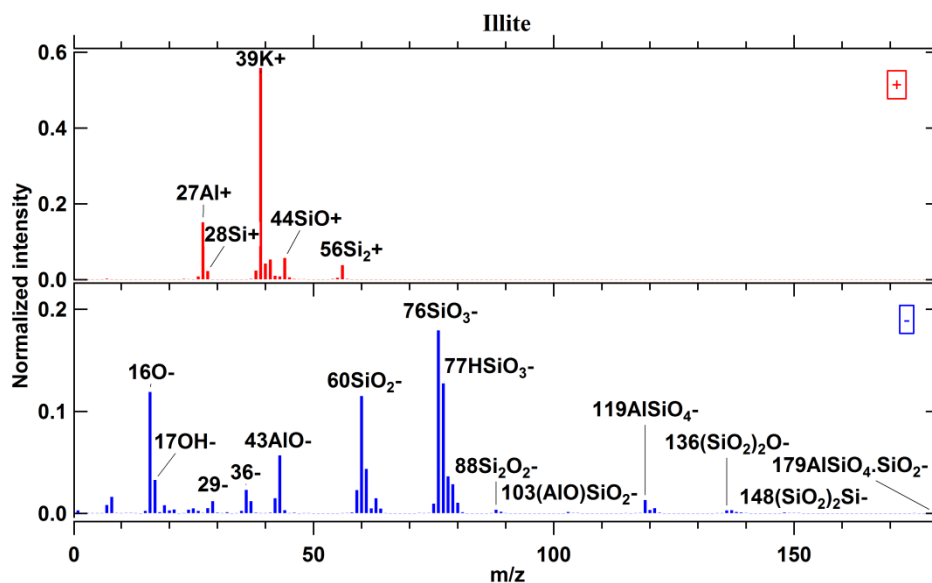
Figure S12: Average mass spectra for illite particles, 807 single spectra averaged

Illite particles, mainly containing aluminosilicates, showed signatures for potassium (m/z 39 K^+ and 41 K^+), alumina (m/z 27 Al^+, 43 AlO^-, and 59 AlO_2^-), silica (m/z 28 Si^+, 44 SiO^+, 56 Si_2^+, 60 SiO_2^-, 76 SiO_3^-, 77 $HSiO_3^-$, 136 $(SiO_2)_2O^-$, and 148 $(SiO_2)_2Si^-$), and oxides of aluminium and silicon (m/z 119 $AlSiO_4^-$, and 179 $AlSiO_4.SiO_2^-$). The K/Si ratio is ~25, which is comparable to this ratio observed in Illite spectra measured by PALMS (Zawadowicz et al., 2017).

91
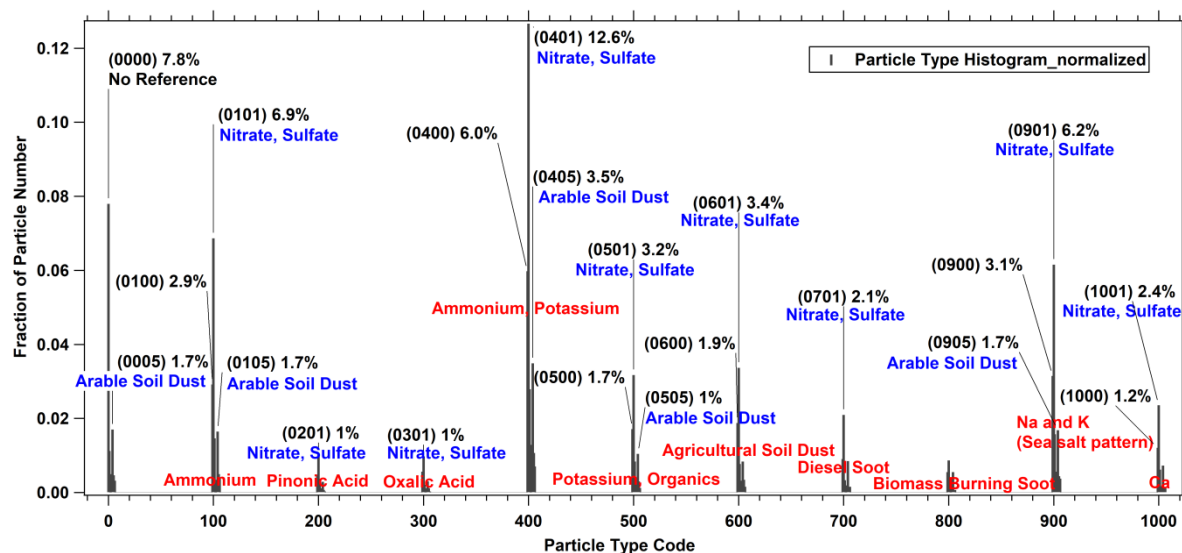
92 **Figure S13: Particle type histogram based on the classification of field data (on July 29th, 2016 during TRAM01 campaign) according**
93 **to laboratory-based reference spectra. The numbers in the brackets are the combination of positive (the front two digits) and negative**
94 **codes (the rear two digits) for reference particles, which are listed in Table S3. There are 11 clusters in this plot with 10 positive**
95 **references labelled in red texts, while the corresponding negative references are labelled in blue texts beneath the corresponding**
96 **codes.**

97

Procedures for LAAPTOF data analysis with an emphasize on mass calibration

1. Open two Igor experiments, using the same raw data (One is for comparison, another is for further analysis)

2. In one Igor experiment: go through the raw spectra (e.g. from the negative spectra, m/z 1, 16 and 17, 24, 25 and 26 are easier to be recognized), to find out the possible fragments, with the help of peak assignments in Table 1 as well as the laboratory based reference spectra.

3. In another Igor experiment

   - Setting the First-tof, base line, and remove the empty spectra
   - Start mass calibration

   Step1: Choose 3 masses with relative bigger distance for positive and negative spectra for basic calibration, respectively.

   (Tips: it is better to choose the corresponding positions for such masses in the spectrum # -1 after pressing the tab "Display spectrum", which give us the stack spectra showing the shift, thus help us better locate the mass; double check the mass values referring to the other Igor experiment with only raw data)

   Step2: Exact calibration, by using more masses.

   (Tips: use only values which are certain)

   Step3: Generate and check the average spectra, then adjust mass calibration by experience and comparing with the individual spectrum.

   (Tips: If we have done good mass calibration, the resulting average spectra will be representative, which can help to find more fragments including reasonable patterns like m/z 24^-, 25^-, and 26^- as well as some expected small fragments like m/z 119^- in mineral dust, thus can modify the exact calibration table. Otherwise, we should redo mass calibration from step 1)

   Step4: Plot ptof vs masses for mass calibration, then use power fit to see whether the value is around 0.5, if yes, then the mass calibration is ok.

   Step5: If the data is poly dispersed, we can also use fuzzy classification to double check the mass calibration.

   (Tips: If we have good mass calibration, the fuzzy results will be good, namely the real number of output classes can finally (almost) equal to the input class number)

4. Generate average spectra that are normalized to the sum of ion intensities

5. Fuzzy Clustering

   For poly-dispersed particles, we can use Fuzzy classification method. The most important input parameter is the number of classes. We can start from the bigger value (e.g. 20) to the smaller one, until the reasonable number and corresponding classes are found. In this study 6 classes have been found by using this method.

   (Tips: similar classes would be observed if the input number of classes is too big, and the good situation is that the resulting number of classes we found is equal to the input number, which is 6 in this study. In addition, the resulting number of classes with clearly different features strongly depends on the experience of the operating scientist to identify them.)

It should be noted that there is problematic peak shift regarding to the mass calibration, mainly due to the interaction position of the individual particles with the excimer laser beam. Peak shifting problem cannot be completely solved even after aforementioned serious mass calibration.

Procedures for reference spectra-oriented grouping of mass spectra

1. Prepare normalized (to sum) stick spectra from the field data, as well as the reference spectra
2. Correlate each spectrum to the references
3. Define particle type by using Pearson's correlation coefficients (r)

    For each particle, find out the maximum r for both positive and negative spectra, and corresponding particle codes (e.g. 00 to 32 at first; 00 represents that this particle does not correlate with any reference). Each spectrum belongs to only one type.
4. Reduce the number of references by observing the histogram of particle types, in order to minimize the complexity caused by excessive meticulous classification.
5. Repeat step 1 to 3
6. Group particles into different types

    Make histogram of particle types and find out the main ones, then make average spectra for the types chosen and compare them, and redefine particle types.

The equation (S1) for calculating Pearson's correlation coefficients between two waves A and B (e.g. ambient and reference spectrum)

$$r = \frac{\sum_{i=0}^{n-1}(waveA[i]-A)(waveB[i]-B)}{\sqrt{\sum_{i=0}^{n-1}(waveA[i]-A)^2 \sum_{i=0}^{n-1}(waveB[i]-B)^2}}$$

(S1)

Here A is the average of the elements in wave A, B is the average of the elements of wave B and the sum is over all wave elements. Although we mainly discuss the main peaks with higher intensities, in this paper, it is should be mentioned that the bias by the peak intensity in calculating r are inevitable, namely high intensive peaks dominate the value of r. Of course this intensity bias can be reduced by selecting specific mass ranges for the correlation.

Uncertainties for reference-oriented method for grouping mass spectra

In order to estimate the uncertainty for reference-oriented method, we have calculated the relative difference between the highest and the second highest Pearson's correlation coefficients (r1 and r2) for each particle, according to equation (S2):

$$\text{Relative Difference} = \frac{r1-r2}{r1} = \frac{r1_{pos} \times r1_{neg} - r2_{pos} \times r2_{neg}}{r1_{pos} \times r1_{neg}} \qquad (S2)$$
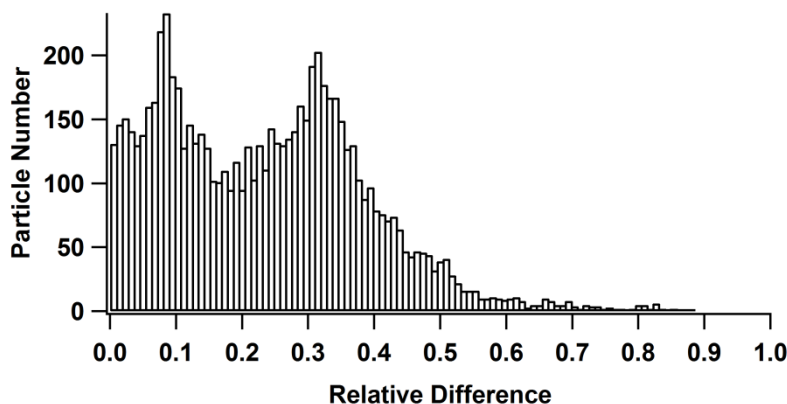
Figure S14: Histogram of relative difference between the highest and the second highest Pearson's correlation coefficient values for each particle measured in the field (on July 29th, 2016 during TRAM01 campaign).

The corresponding statistic calculation results for such relative difference data are listed as follows:

V_npnts= 7314; V_numNaNs= 0; V_numINFs= 0; V_avg= 0.234484;

V_Sum= 1715.02; V_sdev= 0.152986; V_sem= 0.00178885;

V_rms= 0.279972; V_adev= 0.126782; V_skew= 0.595888;

V_kurt= 0.244212; V_minloc= 2005; V_maxloc= 5211;

V_min= 4.35069e-05; V_max= 0.882732; V_minRowLoc= 2005;

V_maxRowLoc= 5211; V_startRow= 0; V_endRow= 7313;

The relative difference mentioned above provides information about the uncertainties for using the reference-spectra oriented method, namely, the bigger the difference is, the smaller the uncertainty will be. It turns out that 77% of the 7314 particles we measured have more than 10% relative difference between r1 and r2, therefore such classification method is reasonable to be used.

There are some factors that could have impact on the uncertainties: 1) the most important one is selection of reference spectra, since two similar references such German soil dust SDGe01 and SDPA01 will lead to similar r that cause little relative difference between r1 and r2 corresponds to higher uncertainty. 2) Peak intensities and mass ranges selected will influence the r values. Bias by peak intensities leads to higher uncertainties whereas well selected mass ranges can also reduce the uncertainties.

Seeking lead (Pb) containing particles using the reference-spectra oriented method

In order to pick out the lead-containing particles, we firstly check the fuzzy results by correlating them to all the reference spectra in the size range of 200 to 220. As shown in Figure S15, all the classes except class 5 have significant correlation with the lead-containing urban dust particles (NIST), which can also be seen in Figure S16 where the corresponding spectra are stacked, showing clear comparable data points in the m/z range of 200 to 220. For Class 5, there are some points offset, leading to lower r, although it also shows similar shape in such m/z range. In the future we will modify our procedure to do better mass calibration and avoid the offset/error data points to solve such problem. Anther problematic issure, which cannot completly solved at present, is the peak shifting mentioned before, expecially for the fragments with bigger mass, such as lead. This will make data interpretation more difficult. In the next step, we correlate each spectrum with the urban dust particles in the m/z range of 200 to 220, and the Pb-containing particles can be selected based on the criteria of r>=0.6. As a result, 55 Pb-containing particles have been found among 7314 particles in the ambient data. Of course also other specific particles can be found using suitable reference spectra.
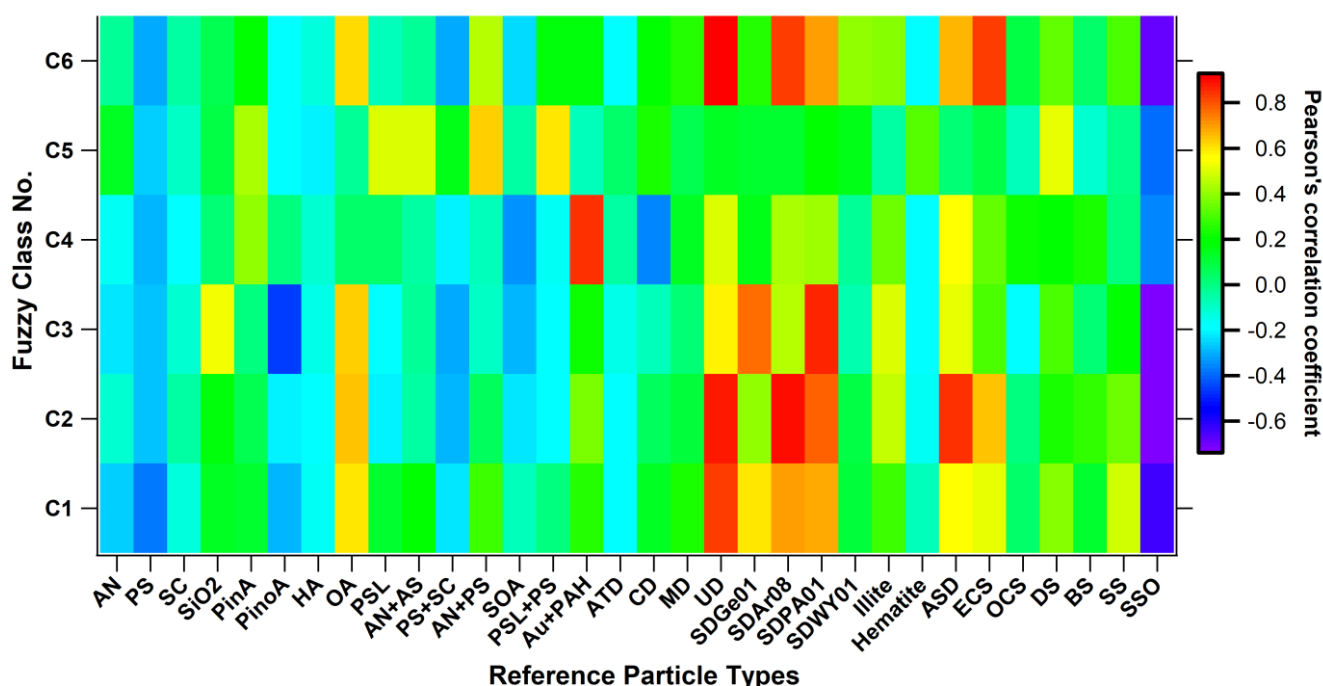
Figure S15: Correlation between fuzzy classification results (6 classes, C1 to C6) and laboratory-based reference spectra only in the m/z range of 200 to 220 for the positive spectra. AN is short for ammonium nitrate, PS-potassium sulfate, SC-sodium chloride, PinA-pinic acid, Pino-pinonic acid, HA-humid acid, OA-oxalic acid, ATD-Arizona test dust, CD-Cairo dust, MD-Morroco dust, UD-urban dust, SDGe01 and SDPA01-soil dusts sampled at two sites from Germany, SDAr08- soil dust from Argentina, SDWY01-soil dust from Wyoming in USA, ASD-agricultural soil dust, ECS-EC rich soot1, OCS-OC rich soot1, DS- diesel soot, BS- biomass burning soot, which is the lignocellulosic char from Chestnut wood, SS-pure sea salt, SSO-sea salt with organics.
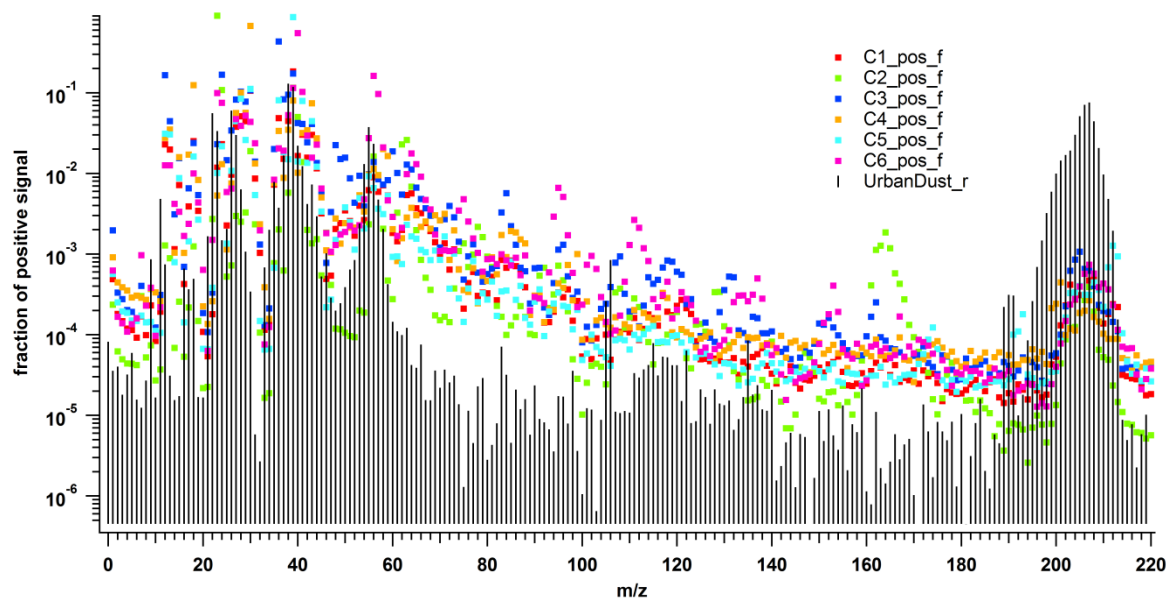
Figure S16: Stacked mass spectra for urban dust particles (NIST) and 5 classes of particles measured on July 29th, 2016 during the field campaign TRAM01.

References

Gallavardin, S., Lohmann, U., and Cziczo, D.: Analysis and differentiation of mineral dust by single particle laser mass spectrometry, Int J Mass Spectrom, 274, 56–63, 2008.

Zawadowicz, M. A., Froyd, K. D., Murphy, D., and Cziczo, D. J.: Improved identification of primary biological aerosol particles using single particle mass spectrometry, Atmos Chem Phys, 17, 7193–7212, 2017.